

Quantum Entanglement, Stratified Spaces, and Topological Matter: Towards an Entanglement-Sensitive Langlands Correspondence

Kazuki Ikeda^{1, 2, *} and Steven Rayan^{3, 4, †}

¹*Department of Physics, University of Massachusetts Boston, Boston, MA 02125, USA*

²*Center for Nuclear Theory, Department of Physics and Astronomy,
Stony Brook University, Stony Brook, New York 11794-3800, USA*

³*Centre for Quantum Topology and Its Applications (quanTA),
University of Saskatchewan, Saskatoon, Saskatchewan S7N 5C9, Canada*

⁴*Department of Mathematics and Statistics, University of Saskatchewan, Saskatoon, Saskatchewan S7N 5E6, Canada*

Recently, quantum entanglement has been presented as a cohomological obstruction to reconstructing a global quantum state from locally compatible information, where sheafification provides a functor that is forgetful with regards to global-from-local signatures while acting faithfully with respect to within-patch multipartite structures. Nontrivial connections to Hecke modifications and the geometric Langlands program are explored in the process. The aim of this work is to validate and extend a number of the claims made in [1] through both theoretical analysis and numerical simulations, employing concrete perspectives from condensed matter physics.

I. Introduction

Quantum entanglement is now a central theme across condensed matter theory, quantum computing and information. In topological materials, much of the progress has come from geometric viewpoints that treat families of ground states as bundles over parameter spaces and use tools such as Berry curvature and Chern numbers to diagnose robust features [2–4]. These constructions usually assume that the parameter space is a smooth manifold on which one can choose global frames up to gauge. In realistic models, this assumption fails precisely where the energy gap closes. At such points the bundle data becomes singular and any attempt to patch local data into a single global description runs into genuine obstructions tied to entanglement. One motivation for dealing directly with this phenomenon is the advent of geometrically-enhanced models for quantum condensed matter, such as the Bloch–bundle picture appearing in *hyperbolic band theory*. Here, tight-binding models on negatively curved (hyperbolic) lattices lead to higher-genus position spaces and higher-dimensional Brillouin-zone analogues [5–9]. Hyperbolic crystallography provides the complementary notion of unit cells and Bravais lattices in this setting [10], while the associated hyperbolic Bloch transform furnishes the relevant noncommutative harmonic analysis [11]. The opportunities for such degenerations of the gap are more plentiful here considering the higher-dimensional nature of Brillouin zone. Very recently, superconducting-circuit experiments have begun to probe these ideas in the laboratory, beginning with [12] in genus 2 and more recently with [13], which to our knowledge realizes for the first time a hyperbolic lattice whose unit cell has genus 3. These experiments enable direct physical realizations and spectral tests of this

non-Euclidean band theory, increasing the relevance of understanding in both mathematical and physical terms the consequences of these potential singularities.

The language of stratified spaces provides a natural way to organize this situation. One regards the parameter space as a union of smooth strata separated by a locus where bands touch. On each regular stratum standard geometric objects are well defined and gauge choices can be made locally. When a path crosses the singular set, topological indices can change in quantized steps and certain coherent features of the state must be modified. This point of view captures the practical fact familiar from band theory and also matches recent mathematical proposals that interpret entanglement as a cohomological obstruction to reconstructing a global state from locally compatible data [1, 14].

In this work, we test and extend that obstruction picture in a concrete condensed-matter setting. We adopt the Haldane model on the honeycomb lattice as a minimal platform with a tunable mass and complex next-nearest neighbor hopping, and we use twisted boundary phases to traverse a two-dimensional torus of boundary conditions. The gap-closing set defines the singular stratum, while the remaining regions form regular strata on which Berry geometry and discretized Chern number are computed reliably. This allows us to study how entanglement signatures track the stratified structure and how quantized responses change when paths cross the singular locus.

A key technical element is the use of entanglement witness filtering that isolates the coherence between sublattices within the single-particle sector. (See [15–18] for entanglement witness.) In the single-orbital case this reduction identifies a two-qubit structure at each crystal momentum and leads to exact lattice identities that relate sector-resolved integrals to the Chern number. We show how two or three carefully chosen witnesses reconstruct the full graded response, which we verify numerically on fine Fukui-Hatsugai-Suzuki meshes [19]. We then extend

* kazuki.ikeda@umb.edu

† rayan@math.usask.ca

the construction to multi-orbital embeddings where the curvature-weighted coherence becomes a matrix. The resulting tomography of the matrix is demonstrated by basis probes that recover each matrix element without ambiguity. We also introduce an S -filtered version of the quantum geometric tensor (QGT) and of the quantum Fisher information (QFI). These filtered quantities separate coherent contributions selected by the witness from population effects and obey sharp bounds that tie metrological sensitivity to sublattice entanglement. We validate these bounds numerically and show that large filtered responses concentrate near Dirac vicinities, in agreement with the stratified-space picture where geometry is enhanced near the singular set.

Our analysis supports the claim that entanglement behaves as a global-from-local obstruction whose strength and location are controlled by the stratification of parameter space. The Haldane model provides a testbed where these ideas can be checked against numerics with high precision. The framework developed here is portable to broader classes of band structures and offers a route to combine topological diagnostics with controlled probes of coherence that are sensitive to how the parameter space decomposes into strata.

Although we work with pure, Abelian bands in the Haldane model, the construction extends naturally. For mixed states, one can replace the Berry connection and QGT by the Uhlmann connection [20] and Bures metric [21]. The same witness filter then isolates the entanglement-sensitive part of the Uhlmann phase and mixed-state QFI, and its jumps across stratification walls should again be captured by Hecke modification. For non-Abelian bands with degeneracies, the witness sign S reduces the structure group $U(N)$ to a Levi subgroup L , so that non-Abelian Wilson loops and Hecke modifications act on matrix-valued responses.

This paper is organized as follows. In Sec. II, we recall the stratified space framework with sector projectors and duality. In Sec. III we explore entanglement across a stratified space associated with the Haldane model. Sec. IIIA describes our setup. Sec. IIIB derives exact lattice identities for the sector integrals ν_{\pm} and for the graded response ν , and verifies them across the phase diagram. Sec. IIIC extends the construction to multiple orbitals, defines the matrix-valued curvature-weighted coherence J_F , and demonstrates reconstruction of J_F along with the Levi-type classification of S . In Sec. IV, we introduce the S -filtered QFI and QGT, and explore its relation to the conventional QFI and QGT. Sec. V concludes and outlines future directions.

II. Framework on a Stratified Parameter Space

A. Quantum Entanglement Index

We consider quantum many-body systems on the parameter manifold $X = T_{\Phi}^2 \times \mathbb{R}_M$ and the gap-closing

set

$$\Sigma = \{(\Phi, M) \in X : \Delta(\Phi; M) = 0\}, \quad (1)$$

where Δ denotes the valence-conduction spectral gap of the family. The open regular part is $X^{\circ} := X \setminus \Sigma$. On X° , the valence bundle $E \rightarrow X^{\circ}$ is smooth and carries the well-known Berry connection A with curvature F_A . Since the adiabatic bundle fails to extend across Σ , global integrals are understood by excision: remove a thin tubular neighbourhood $N_{\varepsilon}(\Sigma)$, integrate on the manifold with boundary $X_{\varepsilon} := X \setminus N_{\varepsilon}(\Sigma)$, and then take $\varepsilon \rightarrow 0$. The boundary contribution supported on $\partial N_{\varepsilon}(\Sigma)$ implements the middle extension $j_{!*}$ that restores quantization.

To relate this to Hecke modifications, choose a two-dimensional slice $C \subset X$ (e.g. a twist torus or a two-parameter plane) which intersects Σ transversely. Then

$$C^{\circ} := C \cap X^{\circ} = C \setminus \{p_a\}, \quad \{p_a\} := C \cap \Sigma, \quad (2)$$

is a punctured surface with a smooth L -bundle $E|_{C^{\circ}} \rightarrow C^{\circ}$. At each intersection point p_a the gap closes and the bundle cannot be extended trivially across p_a . Instead, the phases on the two sides of the gap closing correspond to L -bundles which differ by a Hecke modification of type λ_a at p_a .

Let $W \in \Gamma(\text{End}E)$ be A -parallel ($D_A W = 0$) and set $S := \text{sgn}(W)$. Then $D_A S = 0$ and parallel transport preserves the spectral splitting

$$E = E^+ \oplus E^0 \oplus E^-, \quad S|_{E^{\pm}} = \pm I, \quad S|_{E^0} = 0,$$

so the structure group reduces to the Levi subgroup

$$L \cong U(r_+) \times U(r_-) \times U(r_0), \quad r_{\bullet} = \text{rank } E^{\bullet}. \quad (3)$$

In particular, the S -filtered two-form

$$\Omega^{(S)} = \text{Tr}(S F_A) = \text{Tr}(F_{A_+}) - \text{Tr}(F_{A_-}) \in \Omega^2(X^{\circ}) \quad (4)$$

is globally defined on the reduced bundle and is closed.

For a loop $\gamma \subset X^{\circ}$, let $g_{\pm}(\gamma) = \text{Hol}_{A_{\pm}}(\gamma) \in U(r_{\pm})$ be the block holonomies. The L -character associated to S is

$$\chi_S(\text{Hol}_A(\gamma)) := \det g_+(\gamma) \det g_-(\gamma)^{-1} \in U(1). \quad (5)$$

If $\gamma = \partial C$ for an oriented surface $C \subset X^{\circ}$, one obtains the integer charge

$$\text{Ind}_S|_C := \frac{1}{2\pi} \arg \chi_S(\text{Hol}_A(\gamma)) = \frac{1}{2\pi i} \int_C \Omega^{(S)} \in \mathbb{Z}, \quad (6)$$

which we call the *Quantum Entanglement Index* (QEI) on C .

On the twist torus T_{Φ}^2 , taking A to be the Berry connection and using the single-excitation reduction gives

$$\nu_S = \frac{1}{2\pi} \sum_{\square} F(\Phi) \langle S \rangle_{\Phi} = \frac{1}{2\pi i} \int_{T_{\Phi}^2} \text{Tr}(S F_A), \quad (7)$$

together with the exact sector identities

$$\mu = \nu_+ + \nu_-, \quad \nu = \nu_+ - \nu_- = \nu_S. \quad (8)$$

B. Hecke modifications and entanglement-sensitive Langlands correspondence

Upon complexification, the Levi subgroup (3) becomes

$$L_{\mathbb{C}} \cong GL_{r_+}(\mathbb{C}) \times GL_{r_-}(\mathbb{C}) \times GL_{r_0}(\mathbb{C}). \quad (9)$$

Let $T_L \subset L_{\mathbb{C}}$ be the standard maximal torus consisting of block-diagonal matrices that are diagonal in each GL block. Write $X^*(T_L)$ for the character (weight) lattice and $X_*(T_L)$ for the coweight lattice.

Let C be a compact Riemann surface. A (dominant) *Hecke modification* of type $\lambda \in X_*(T_L)$ at $p \in C$ is defined by gluing with the transition function $g_{\lambda}(z) = z^{\lambda} \in L$ over a small disc D centered at p :

$$E'|_D \simeq E|_D, \quad E'|_{C \setminus D} \simeq E|_{C \setminus D},$$

glued along ∂D by g_{λ} .

Writing $\lambda = \text{diag}(\lambda^+, \lambda^0, \lambda^-)$ in the L -adapted frame with integer diagonal entries, one has

$$\deg(\det E'^{\pm}) = \deg(\det E^{\pm}) + \sum_i \lambda_i^{\pm}.$$

The S -index on C can be written as

$$\text{Ind}_S|_C = \deg(\det E^+) - \deg(\det E^-).$$

Under a Hecke modification of type λ at p ,

$$\Delta \text{Ind}_S|_{\{p\}} = \left(\sum_i \lambda_i^+ \right) - \left(\sum_j \lambda_j^- \right) =: \langle S, \lambda \rangle, \quad (10)$$

and additively for multiple points $\{p_a\}$,

$$\Delta \text{Ind}_S|_C = \sum_a \langle S, \lambda_a \rangle, \quad (11)$$

corresponding to the total change of the QEI along C when passing through the gap closings.

Physically, each time a path in parameter space crosses the gap-closing stratum Σ (eq. (1)), the valence bundle undergoes a Hecke modification at the intersection point, and the corresponding weight-coweight pairing encodes the quantized jump of the Chern number or entanglement response. In this sense the gap-closing locus is precisely the support of the Hecke modification ('t Hooft-type defect) in the stratified parameter space, while the Wilson-Hecke correspondence gives a geometric Langlands interpretation of topological phase transitions in condensed matter systems [22, 23]. In our construction, this correspondence is intrinsically quantum: the relevant Hecke weight (charge) is selected by quantum entanglement, in the sense that the weight entering the pairing is the Levi character χ_S determined by the spectrum of the entanglement witness $S = \text{sgn}(W)$ (see Sections III B and III C for a detailed analysis of the Haldane model). We therefore refer to this duality as a *entanglement-sensitive Langlands correspondence* [1].

The correspondence is summarized in the table below; there, the Wilson loop observable is the L -character (5), whose phase is the integrated S -weighted curvature (6). The Hecke modification of type λ produces the quantized jump (10) in conductance (topological charge).

Electric (Wilson)	Magnetic (Hecke)
L -character $\chi_S = \det g_+ \det g_-^{-1}$	Cocharacter $\lambda \in X_*(L)$
Phase $\arg(\chi_S) = \int \text{Tr}(SF_A)$	Jump $\Delta \text{Ind}_S = \langle S, \lambda \rangle$

III. Haldane model

A. Setup

We work with the spinless Haldane model [24] with two orbitals (A/B) per unit cell. Let $a_{\mathbf{r}}$ and $b_{\mathbf{r}}$ annihilate a fermion on the A and B sites of unit cell \mathbf{r} . The tight-binding Hamiltonian with real nearest-neighbour (NN) hopping t_1 , complex next-nearest-neighbour (NNN) hopping $t_2 e^{i\varphi}$ carrying zero net flux per unit cell, and sublattice staggering M is

$$\begin{aligned} H = & t_1 \sum_{\mathbf{r}} \sum_{m=1}^3 (a_{\mathbf{r}}^\dagger b_{\mathbf{r}+\delta_m} + \text{h.c.}) \\ & + t_2 \sum_{s \in \{A, B\}} \sum_{\mathbf{r} \in s} \sum_{j=1}^3 e^{i\nu_s(\mathbf{b}_j) \varphi} c_{\mathbf{r}}^\dagger c_{\mathbf{r}+\mathbf{b}_j} \\ & + M \sum_{\mathbf{r}} (a_{\mathbf{r}}^\dagger a_{\mathbf{r}} - b_{\mathbf{r}}^\dagger b_{\mathbf{r}}), \end{aligned}$$

where $c_{\mathbf{r}}$ stands for $a_{\mathbf{r}}$ on A and $b_{\mathbf{r}}$ on B, the unit vectors $\{\delta_m\}$ connect NN sites, $\{\mathbf{b}_j\}$ connect NNN sites within the same sublattice, and the orientation factor satisfies $\nu_A(\mathbf{b}_j) = +1$, $\nu_B(\mathbf{b}_j) = -1$ for a fixed clockwise convention on the two triangular sublattices. This choice breaks time-reversal symmetry without a net magnetic field and produces opposite effective fluxes on A and B.

With

$$\delta_1 = (0, 1), \quad \delta_2 = \left(-\frac{\sqrt{3}}{2}, -\frac{1}{2} \right), \quad \delta_3 = \left(\frac{\sqrt{3}}{2}, -\frac{1}{2} \right),$$

and oriented NNN differences $\{\mathbf{b}_j\}_{j=1}^3$, the 2×2 Bloch Hamiltonian is

$$\begin{aligned} h_{\mathbf{k}} &= d_0(\mathbf{k}) I_2 + d(\mathbf{k}) \cdot \sigma, \\ d_x(\mathbf{k}) + id_y(\mathbf{k}) &= t_1 \sum_{m=1}^3 e^{i\mathbf{k} \cdot \delta_m}, \\ d_0(\mathbf{k}) &= 2t_2 \cos \varphi \sum_{j=1}^3 \cos(\mathbf{k} \cdot \mathbf{b}_j), \\ d_z(\mathbf{k}) &= M - 2t_2 \sin \varphi \sum_{j=1}^3 \sin(\mathbf{k} \cdot \mathbf{b}_j). \end{aligned} \quad (12)$$

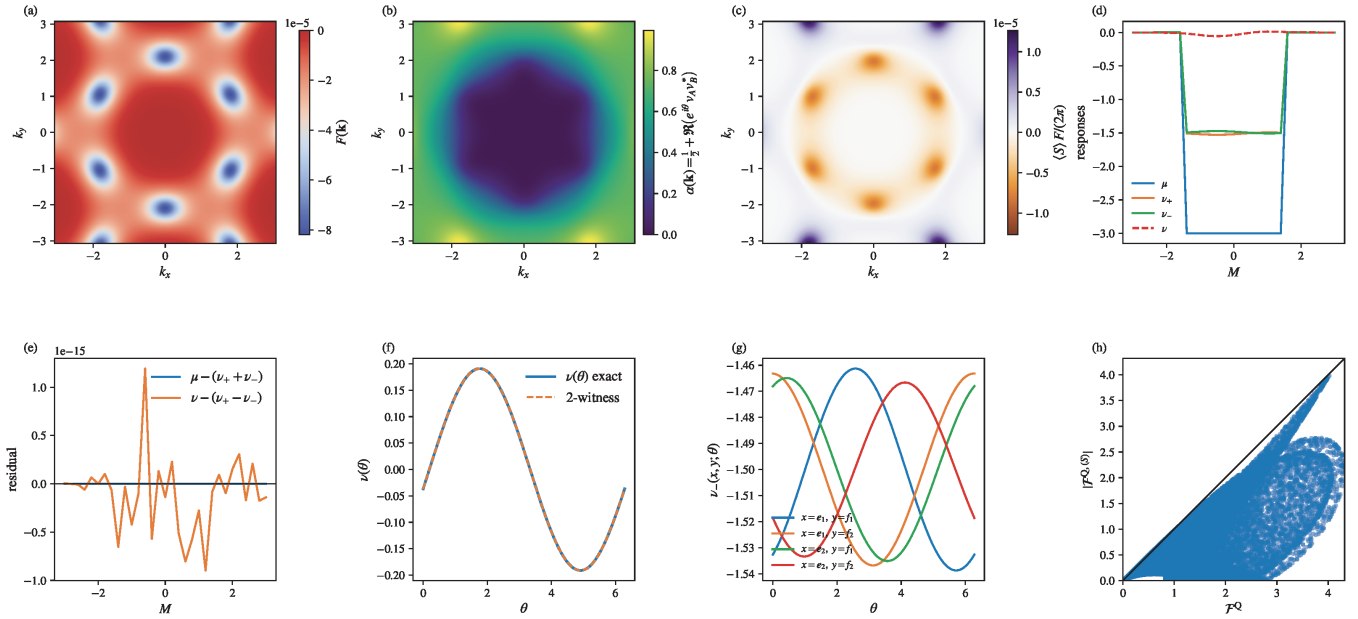


FIG. 1: (a) FHS curvature $F(\mathbf{k})$; its sum yields the Chern number $\mu = \frac{1}{2\pi} \sum_{\mathbf{k}} F(\mathbf{k})$. (b) $\alpha(\mathbf{k}; \theta) = \frac{1}{2} + \text{Re}(e^{i\theta} v_A v_B^*)$. (c) Graded density $\langle S \rangle F/(2\pi)$ with $\langle S \rangle = 1 - 2\alpha$; its sum is the graded response $\nu(\theta)$. (d) $\mu(M)$, $\nu_{\pm}(M)$ and $\nu(M) = \nu_+(M) - \nu_-(M)$, confirming the discrete identities $\mu = \nu_+ + \nu_-$ and $\nu = \nu_+ - \nu_-$. The quantized jumps of these responses at the critical values of M coincide with the crossings of the gap-closing stratum Σ and realize the Hecke jumps ΔInd_S along this path. (e) Residuals $r_{\mu} = \mu - (\nu_+ + \nu_-)$ and $r_{\nu} = \nu - (\nu_+ - \nu_-)$, confirmed to be negligibly small, on the order of 10^{-15} . (f) Tomography (reconstruction of J_F): exact $\nu(\theta) = -2 \text{Re}(e^{i\theta} J_F^{AB})$ against the two-witness reconstruction from $\theta = 0, \pi/2$, where $J_F^{AB} = \frac{1}{2\pi} \sum_{\mathbf{k}} F v_A v_B^*$. (g) Multi-orbital samples: $\nu_-(x, y; \theta) = \frac{\mu}{2} + \text{Re}(e^{i\theta} x^{\dagger} J_F y)$ with $J_F = \frac{1}{2\pi} \sum_{\mathbf{k}} F a b^{\dagger}$ for the embedding $a = v_A x$, $b = v_B y$. (h) S -filtered QFI inequality: $\mathcal{F}^Q = 4g_{ii}$ and $\mathcal{F}^{Q,(S)} \leq 4 \|P^{\perp} S' P^{\perp}\| g_{ii} \leq \mathcal{F}^Q$. Here, all random scatter points lie below the line $y = x$.

On an $N_x \times N_y$ torus obtained by the Fukui-Hatsugai-Suzuki (FHS) discretization [19], the link variables and plaquette curvature are

$$U_{\alpha}(\mathbf{k}) = \frac{\langle u_-(\mathbf{k}) | u_-(\mathbf{k} + \hat{\alpha}) \rangle}{|\langle u_-(\mathbf{k}) | u_-(\mathbf{k} + \hat{\alpha}) \rangle|}, \quad (13)$$

$$F(\mathbf{k}) = \arg \left[\frac{U_x(\mathbf{k}) U_y(\mathbf{k} + \hat{x})}{U_x(\mathbf{k} + \hat{y}) U_y(\mathbf{k})} \right].$$

Using these we obtain the invariant $\mu = \frac{1}{2\pi} \sum_{\square} F(\mathbf{k})$ (8). At the Dirac points K, K' , the effective masses are

$$m_K = M - 3\sqrt{3} t_2 \sin \varphi, \quad m_{K'} = M + 3\sqrt{3} t_2 \sin \varphi,$$

so $\mu = \frac{1}{2} [\text{sgn}(m_K) - \text{sgn}(m_{K'})]$. In Fig. 1 (a), we show the lattice Berry curvature $F(\mathbf{k})$ on the Brillouin zone. Red (blue) regions indicate positive (negative) local Berry flux. Integrating F over the mesh gives the Chern number μ , which exhibits the expected quantized value in the topological phase.

The model realizes a Chern insulator by opening Dirac masses of opposite sign at the inequivalent valleys K, K' via the complex NNN hopping. Inversion symmetry breaking is controlled independently by M .

In the language of Sec. II, the parameter space is the product of the Brillouin torus with model couplings,

$X = T_{\mathbf{k}}^2 \times \mathbb{R}_{(M, t_2, \varphi)}^3$. The gap-closing set $\Sigma = \{m_K = 0\} \cup \{m_{K'} = 0\}$ stratifies X into topological chambers with constant Chern number. Crossings of Σ implement the magnetic (Hecke) jumps of the index. On $X^{\circ} = X \setminus \Sigma$, the valence bundle is smooth and the witness $S = \text{sgn}(W)$ reduces the structure group to the Levi subgroup. As we discuss in the next subsection, in the single-orbit Haldane case, the single-excitation sector $S_1 = \text{span}\{|01\rangle, |10\rangle\}$ has $(r_+, r_-, r_0) = (1, 1, 0)$, so $L \simeq U(1) \times U(1)$. The associated L -character $\chi_S(g_+, g_-) = \det g_+ \det g_-^{-1}$ evaluates the entanglement Wilson loop, and the filtered curvature $\Omega(S) = \text{Tr}(S F_A)$ integrates to the same lattice charge measured by ν_S on $T_{\mathbf{k}}^2$. Thus, the standard Chern phase diagram of the Haldane model is an explicit example of our stratified-space picture and of the Levi reduction induced by an entanglement witness.

B. Single orbit case

Let $\mathcal{H}_{\text{Bloch}} \cong \mathbb{C}^2$ with basis $\{|A\rangle, |B\rangle\}$ and, at fixed \mathbf{k} ,

$$\mathcal{H}_{\mathbf{k}} = \text{span}\{|00\rangle\} \oplus \mathcal{S}_1(\mathbf{k}) \oplus \text{span}\{|11\rangle\}, \quad (14)$$

$$\mathcal{S}_1(\mathbf{k}) = \text{span}\{|01\rangle, |10\rangle\}.$$

If $|u_-(\mathbf{k})\rangle = v_A(\mathbf{k})|A\rangle + v_B(\mathbf{k})|B\rangle$ then the canonical isometry $\mathcal{J} : \alpha|A\rangle + \beta|B\rangle \mapsto \alpha|10\rangle_{\mathbf{k}} + \beta|01\rangle_{\mathbf{k}}$ gives the ground-state one-particle spinor

$$|\Psi_{\mathbf{k}}\rangle = \mathcal{J}|u_-(\mathbf{k})\rangle = v_A(\mathbf{k})|10\rangle_{\mathbf{k}} + v_B(\mathbf{k})|01\rangle_{\mathbf{k}}, \quad (15)$$

$$\rho_{\mathbf{k}} = |\Psi_{\mathbf{k}}\rangle\langle\Psi_{\mathbf{k}}| = P_1\rho_{\mathbf{k}}P_1,$$

with $P_1 = |01\rangle\langle 01| + |10\rangle\langle 10|$. Writing $\hat{\mathbf{n}}(\mathbf{k}) = d/\|d\|$ and $P_v = (I - \hat{\mathbf{n}} \cdot \sigma)/2$, we have

$$|v_A|^2 = \langle A|P_v|A\rangle = \frac{1-\hat{n}_z}{2}, \quad |v_B|^2 = \frac{1+\hat{n}_z}{2}, \quad (16)$$

$$v_A v_B^* = \langle A|P_v|B\rangle = \frac{-\hat{n}_x+i\hat{n}_y}{2}.$$

Let $\rho^{T_B} = \frac{1}{N} \sum_{\mathbf{k}} \rho_{\mathbf{k}}^{T_B}$ and define

$$z = \langle v_B(\mathbf{k}) v_A(\mathbf{k})^* \rangle_{\mathbf{k}}, \quad \theta = \arg z.$$

Take $W = (|w_-\rangle\langle w_-|)^{T_B}$ with $|w_-\rangle = \frac{1}{\sqrt{2}}(e^{-i\theta/2}|00\rangle - e^{+i\theta/2}|11\rangle)$. Then $S = \text{sgn}(W)$ is block-diagonal and, on \mathcal{S}_1 , we have

$$S\Big|_{\mathcal{S}_1} = -\begin{pmatrix} 0 & e^{i\theta} \\ e^{-i\theta} & 0 \end{pmatrix}, \quad |\xi_-\rangle = \frac{1}{\sqrt{2}}(|01\rangle + e^{-i\theta}|10\rangle), \quad (17)$$

with the projector $P_- = |\xi_-\rangle\langle\xi_-|$, $P_+ = I - P_-$. Because $\rho_{\mathbf{k}} = P_1\rho_{\mathbf{k}}P_1$, for any X we have $\text{Tr}(X\rho_{\mathbf{k}}) = \text{Tr}((P_1XP_1)\rho_{\mathbf{k}})$. Hence only the 2×2 block on \mathcal{S}_1 contributes. Define the curvature-weighted coherence as

$$J_F^{AB} = \frac{1}{2\pi} \sum_{\square} F(\mathbf{k}) v_A(\mathbf{k}) v_B(\mathbf{k})^*,$$

and the weight at \mathbf{k} by

$$\alpha(\mathbf{k}) = \langle \Psi_{\mathbf{k}} | P_- | \Psi_{\mathbf{k}} \rangle = \frac{1}{2} + \text{Re}(e^{i\theta} v_A v_B^*), \quad (18)$$

$$\langle \Psi_{\mathbf{k}} | S | \Psi_{\mathbf{k}} \rangle = 1 - 2\alpha(\mathbf{k}).$$

Fig. 1 (b) displays $\alpha(\mathbf{k}) = \frac{1}{2} + \text{Re}(e^{i\theta_{\text{ref}}} v_A(\mathbf{k}) v_B(\mathbf{k})^*)$, which measures the local A/B coherence of the occupied spinor with a reference phase θ_{ref} . Bright regions correspond to constructive A/B interference (larger Re), dark regions to destructive interference.

Exact FHS sums give

$$\nu_-(W) = \frac{1}{2\pi} \sum_{\square} \alpha F = \frac{\mu}{2} + \text{Re}(e^{i\theta} J_F^{AB}),$$

$$\nu_+(W) = \frac{\mu}{2} - \text{Re}(e^{i\theta} J_F^{AB}), \quad (19)$$

$$\nu_S = \frac{1}{2\pi} \sum_{\square} \langle \Psi_{\mathbf{k}} | S | \Psi_{\mathbf{k}} \rangle F = \nu_+ - \nu_-.$$

The product $\langle S \rangle F$ weighs the curvature by the witness, as shown in Fig. 1 (c). Integrating this panel over the Brillouin zone yields the graded response ν_S . For each M we also plot the sector responses ν_{\pm} and the graded response ν in panel (d). As M crosses the gap-closing values, the valence bundle on the slice C° (eq. (2)) undergoes

a Hecke modification and the indices μ, ν_{\pm}, ν exhibit the predicted quantized jumps. Then we quantify the identities in (d) by plotting $\mu - (\nu_+ + \nu_-)$ and $\nu_{\text{ref}} - (\nu_+ - \nu_-)$ in panel (e). Residuals are negligibly small (typically on the order of 10^{-15}), confirming that the equalities are satisfied discretely on the FHS grid. Moreover, for a reference mass M_0 , we sweep the witness phase θ and plot $\nu(\theta)$ in panel (f), where the solid curve is the direct evaluation and the dashed curve is the two-witness reconstruction obtained from only $\nu_-(0)$ and $\nu_-(\frac{\pi}{2})$ via $J_F^{AB} = (\nu_-(0) - \frac{1}{2}\mu) - i(\nu_-(\frac{\pi}{2}) - \frac{1}{2}\mu)$. The agreement confirms that J_F^{AB} is fully captured by two phase settings.

In the spinless Haldane model with the A/B mode bipartition and a single particle per k , S restricted to $\mathcal{S}_1 = \text{span}\{|01\rangle, |10\rangle\}$ has eigenvalues $\{\pm 1\}$, so $(r_+, r_-, r_0) = (1, 1, 0)$ and $L \simeq U(1) \times U(1)$. In a convenient gauge $S = \text{diag}(+1, -1)$ on $E^+ \oplus E^-$. The electric side is

$$\frac{1}{2\pi i} \int_C (\text{Tr} F_{A+} - \text{Tr} F_{A-}) = c_1(\det E^+) \Big|_C - c_1(\det E^-) \Big|_C,$$

which matches $\text{Ind}_S \Big|_C$ as given by eq. (6). On the magnetic side, a Hecke modification with $\lambda = \text{diag}(\ell_+, \ell_-)$ shifts Ind_S by $\ell_+ - \ell_-$, so an elementary modification in E^{\pm} contributes ± 1 . On the full Fock space, S has spectrum $\{+1, +1, +1, -1\}$, i.e. $(r_+, r_-, r_0) = (3, 1, 0)$, but the extra $+1$ directions live in $\text{span}\{|00\rangle, |11\rangle\}$ and never contribute because $\rho_k = P_1\rho_kP_1$.

C. Multi-orbital case

Let $\dim \mathcal{H}_A = m$, $\dim \mathcal{H}_B = n$ and write

$$|\Psi_{\mathbf{k}}\rangle = \sum_{i=1}^m a_i(\mathbf{k}) |1_i, 0\rangle + \sum_{j=1}^n b_j(\mathbf{k}) |0, 1_j\rangle, \quad (20)$$

$$J_F = \frac{1}{2\pi} \sum_{\square} F(\mathbf{k}) a(\mathbf{k}) b(\mathbf{k})^{\dagger} \in \mathbb{C}^{m \times n}.$$

Here $a(\mathbf{k}) = (a_1(\mathbf{k}), \dots, a_m(\mathbf{k}))^{\top}$ and $b(\mathbf{k}) = (b_1(\mathbf{k}), \dots, b_n(\mathbf{k}))^{\top}$, and we use the single-excitation reduction as before.

At each \mathbf{k} we decompose the two-mode Fock space across the A/B bipartition as

$$\mathcal{H}_{\mathbf{k}} = \text{span}\{|00\rangle\} \oplus \mathcal{S}_1(\mathbf{k}) \oplus \text{span}\{|11\rangle\}, \quad (21)$$

$$\mathcal{S}_1(\mathbf{k}) = \text{span}\{|1_i, 0\rangle\}_{i=1}^m \oplus \text{span}\{|0, 1_j\rangle\}_{j=1}^n.$$

Let P_1 denote the projector onto $\mathcal{S}_1(\mathbf{k})$:

$$P_1 = \sum_{i=1}^m |1_i, 0\rangle\langle 1_i, 0| + \sum_{j=1}^n |0, 1_j\rangle\langle 0, 1_j|.$$

The ground-state one-particle spinor lies entirely in \mathcal{S}_1 , and we consider the density matrix:

$$\rho_{\mathbf{k}} := |\Psi_{\mathbf{k}}\rangle\langle\Psi_{\mathbf{k}}| = P_1 \rho_{\mathbf{k}} P_1.$$

Consequently, for any observable X (in particular for the witness sign $S = \text{sgn}(W)$), only its \mathcal{S}_1 block contributes:

$$\text{Tr}(X\rho_{\mathbf{k}}) = \text{Tr}((P_1XP_1)\rho_{\mathbf{k}}), \quad (22)$$

so we work with

$$S|_{\mathcal{S}_1} = -\begin{pmatrix} 0 & Y \\ Y^\dagger & 0 \end{pmatrix}, \quad (23)$$

where $Y \in \mathbb{C}^{m \times n}$, $Y_{ij} := -\langle 1_i, 0 | S | 0, 1_j \rangle$, and all sector identities below follow from this reduced block. With this convention $Y : \mathcal{H}_B \rightarrow \mathcal{H}_A$ is the off-diagonal block on \mathcal{S}_1 . Since $S = \text{sgn}(W)$ has spectrum $\{+1, 0, -1\}$, the block form above forces Y to be a partial isometry on its support: $Y^\dagger Y$ and YY^\dagger are orthogonal projections of the same rank $r = \text{rank } Y$. With (17), the spectrum of S consists of r copies of $+1$, r copies of -1 , and $(m+n-2r)$ zeros:

$$(r_+, r_-, r_0) = (\text{rank } Y, \text{rank } Y, m+n-2\text{rank } Y), \quad (24)$$

Hence the structure group reduces to the Levi subgroup $U(r) \times U(r) \times U(m+n-2r)$.

Now let us relate these with Sec. II B. The sign splitting $S = \text{sgn}(W)$ selects the L -character

$$\chi_S \in X^*(T_L), \quad \chi_S(g_+, g_0, g_-) = \det(g_+) \det(g_-)^{-1},$$

where $T_L \subset L_{\mathbb{C}}$ is the standard maximal torus (diagonal in each $GL_{r_{\bullet}}$ block). Thus χ_S has weight $+1$ on the E_+ block, weight -1 on E_- , and is trivial on E_0 . A Hecke modification of type $\lambda \in X_*(T_L)$ at a point is given by the loop $g_{\lambda}(z) = z^{\lambda}$ on the affine Grassmannian $\text{Gr}_{L_{\mathbb{C}}}$. The natural weight-coweight pairing

$$\langle \cdot, \cdot \rangle : X^*(T_L) \times X_*(T_L) \longrightarrow \mathbb{Z}$$

recovers the index jump (10):

$$\Delta \text{Ind}_S = \langle \chi_S, \lambda \rangle.$$

Equivalently, if $\lambda = (\lambda_+, \lambda_-, \lambda_0)$ encodes the elementary degree changes in the three blocks, then $\langle \chi_S, \lambda \rangle = \sum_i (\lambda_+)_i - \sum_j (\lambda_-)_j$ (10). This is the electric-magnetic duality in Sec. II B: the Wilson loop determined by χ_S pairs with the coweight λ to produce the quantized jump.

Let ${}^L L$ be the Langlands dual of $L_{\mathbb{C}}$. Since GL_n is self-dual, one has

$${}^L L \simeq GL_{r_+} \times GL_{r_-} \times GL_{r_0}.$$

By general duality,

$$X^*(T_L) \cong X_*({}^L T_L), \quad X_*(T_L) \cong X^*({}^L T_L).$$

Under the (geometric) Satake equivalence for $L_{\mathbb{C}}$,

$$\text{Perv}_{L_{\mathbb{C}}(\mathcal{O})}(\text{Gr}_{L_{\mathbb{C}}}) \simeq \text{Rep}({}^L L),$$

a dominant coweight $\lambda \in X_*(T_L)$ labels the spherical kernel $S_{V_{\lambda}}$ for the Hecke functor $H_{x, V_{\lambda}}$, where V_{λ} is the

irreducible ${}^L L$ representation of highest weight λ . The L -character χ_S corresponds, on the dual side, to a one-dimensional representation $\widehat{\chi}_S \in X^*({}^L L)$. Hence on an $L_{\mathbb{C}}$ -eigensheaf the Hecke functor acts by the scalar

$$\widehat{\chi}_S(\text{Hol}_{L_{\mathbb{C}}}(x)) = \chi_S(\text{Hol}_L(x)) = \det g_+(x) \det g_-(x)^{-1},$$

which is the entanglement Wilson loop W_S of Sec. II. A Hecke modification of type λ multiplies this eigenvalue by $z \langle \chi_S, \lambda \rangle$ and shifts the QEI by $\langle \chi_S, \lambda \rangle$ (10).

For unit vectors $x \in \mathbb{C}^m$, $y \in \mathbb{C}^n$ we abbreviate $|1_{x, 0} \rangle := \sum_i x_i |1_i 0 \rangle$ and $|0, 1_y \rangle := \sum_j y_j |0, 1_j \rangle$. For equal-split rank-1 witnesses

$$|\xi_-(x, y, \theta) \rangle = \frac{1}{\sqrt{2}} (|0, 1_y \rangle + e^{-i\theta} |1_x, 0 \rangle),$$

one has the exact lattice identities

$$\begin{aligned} \nu_-(x, y; \theta) &= \frac{\mu}{2} + \text{Re}(e^{i\theta} x^\dagger J_F y), \\ \nu(x, y; \theta) &= -2 \text{Re}(e^{i\theta} x^\dagger J_F y). \end{aligned} \quad (25)$$

Under local basis changes $U_A \in U(m)$, $U_B \in U(n)$, one has $a \mapsto U_A a$, $b \mapsto U_B b$, $J_F \mapsto U_A J_F U_B^\dagger$, $Y \mapsto U_A Y U_B^\dagger$, and the scalars $x^\dagger J_F y$ (hence ν_{\pm} , ν) are invariant. For $m = n = 1$, J_F is a scalar and (25) reduce to the formulas (19). For several test pairs (x, y) we plot $\nu_{\pm}(x, y; \theta)$ in Fig. 1 (g). With the canonical basis vectors $(e_i, f_j) \in \mathbb{C}^m \times \mathbb{C}^n$ for the A- and B-orbits, we plot $\nu_-(e_i, f_j; \theta) = \frac{\mu}{2} + \text{Re}(e^{i\theta} J_F^{ij})$ in Fig. 1 (g). By scanning (i, j) over the chosen basis, the full matrix J_F is reconstructed.

IV. Relation to Quantum Geometric Tensor and Quantum Fisher Information

A. Definitions

For a smooth family of normalized valence states $|u_-(\lambda) \rangle$ depending on parameters $\lambda = (\lambda^1, \lambda^2, \dots)$, the quantum geometric tensor (QGT) [25] is

$$\mathcal{Q}_{ij} = \langle \partial_i u_- | (I - |u_-\rangle \langle u_-|) \partial_j u_- \rangle = g_{ij} + \frac{i}{2} F_{ij}, \quad (26)$$

where $g_{ij} = \text{Re } \mathcal{Q}_{ij}$ is the Fubini-Study (FS) metric and $F_{ij} = 2 \text{Im } \mathcal{Q}_{ij}$ is the Berry curvature two-form. In a two-band model one may write $P_v = (I - \hat{\mathbf{n}} \cdot \sigma)/2$ with $\hat{\mathbf{n}} = d/\|d\|$ as in (16). A standard computation gives the closed forms

$$g_{ij} = \frac{1}{4} \partial_i \hat{\mathbf{n}} \cdot \partial_j \hat{\mathbf{n}}, \quad F_{ij} = \frac{1}{2} \hat{\mathbf{n}} \cdot (\partial_i \hat{\mathbf{n}} \times \partial_j \hat{\mathbf{n}}). \quad (27)$$

When $(\lambda^1, \lambda^2) = (\Phi_x, \Phi_y)$ are twists on the torus, the FHS discretization used elsewhere in the paper yields $F(\mathbf{k})$ and the Chern number $\mu = \frac{1}{2\pi} \sum_{\square} F(\mathbf{k})$ as eq.(8).

For pure states, the quantum Fisher information (QFI) tensor equals four times the FS metric [26, 27]:

$$\mathcal{F}_{ij}^Q = 4 g_{ij} = 4 \text{Re } \mathcal{Q}_{ij}. \quad (28)$$

Along a one-parameter trajectory $\lambda \mapsto |u_-(\lambda)\rangle$ the single-parameter QFI is $\mathcal{F}^Q(\lambda) = 4g_{\lambda\lambda}$. Thus the imaginary part of \mathcal{Q}_{ij} encodes the Berry curvature F_{ij} — i.e. the topology — while the real part controls the optimal metrological sensitivity (QFI) with regards to variations of the parameters.

Let $S = \text{sgn}(W)$ be the sign endomorphism of a decomposable witness W (constructed as in Sec. II), and let S' denote its Bloch-space representative via the single-excitation isometry. So, on the (A, B) Bloch basis,

$$S' = -\cos \theta \sigma_x + \sin \theta \sigma_y, \quad (29)$$

which matches $S|_{\mathcal{S}_1}$ (17).

Define the S -filtered QGT by inserting S' between projectors onto the orthogonal complement of the valence line:

$$\mathcal{Q}_{ij}^{(S)} := \langle \partial_i u_- | P^\perp S' P^\perp \partial_j u_- \rangle, \quad P^\perp := I - |u_-\rangle\langle u_-|. \quad (30)$$

Because in the two-band case $P^\perp = |u_+\rangle\langle u_+|$ is rank-1,

$$\begin{aligned} P^\perp S' P^\perp &= \langle u_+ | S' | u_+ \rangle P^\perp =: \eta P^\perp, \\ \eta &= \langle u_+ | S' | u_+ \rangle = -\langle u_- | S' | u_- \rangle. \end{aligned} \quad (31)$$

Hence one has the following relations:

$$\begin{aligned} \mathcal{Q}_{ij}^{(S)} &= \eta \mathcal{Q}_{ij}, \quad \text{Im } \mathcal{Q}_{ij}^{(S)} = \frac{\eta}{2} F_{ij}, \\ \mathcal{F}_{ij}^{Q,(S)} &:= 4 \text{Re } \mathcal{Q}_{ij}^{(S)} = \eta \mathcal{F}_{ij}^Q. \end{aligned} \quad (32)$$

Since S' is a unit-norm Pauli combination, $|\eta| \leq 1$. In particular, on the twist torus $(\lambda^1, \lambda^2) = (\Phi_x, \Phi_y)$, summing (32) over FHS plaquettes yields

$$\nu_S = \frac{1}{2\pi} \sum_{\square} \langle S \rangle F = -\frac{1}{\pi} \sum_{\square} \text{Im } \mathcal{Q}_{xy}^{(S)}, \quad (33)$$

which is the witness-filtered Chern response defined and verified in Sec. II (eq. (7)).

Along any one-parameter path $\lambda \mapsto |u_-(\lambda)\rangle$, we define the S -filtered QFI by

$$\mathcal{F}^{Q,(S)}(\lambda) := 4 \text{Re } \mathcal{Q}_{\lambda\lambda}^{(S)} = 4\eta g_{\lambda\lambda}.$$

which is a sensitivity that isolates the contribution supported by the S -selected A/B coherence channel (compare with the sector formulas (19)).

B. Inequalities linking S -filtered QGT/QFI to entanglement

We relate entanglement with bounds of the QGT and QFI that will be useful in analysis and numerics.

1. General bounds for all dimensions.

Since $\|P^\perp S' P^\perp\|_{\text{op}} \leq \|S'\|_{\text{op}} \leq 1$, the Cauchy-Schwarz relation in (30) gives

$$|\mathcal{Q}_{ij}^{(S)}| \leq \|S'\|_{\text{op}} \sqrt{g_{ii} g_{jj}} \leq \sqrt{g_{ii} g_{jj}}.$$

In particular, along any parameter λ ,

$$|\mathcal{F}^{Q,(S)}(\lambda)| = 4 |\text{Re } \mathcal{Q}_{\lambda\lambda}^{(S)}| \leq 4 g_{\lambda\lambda} = \mathcal{F}^Q(\lambda). \quad (34)$$

Thus the S -filtered QFI never exceeds the conventional QFI. As we discuss below, for the single orbit case, this inequality is saturated if and only if the state is maximally entangled. However, in higher local dimension, maximal entanglement is neither necessary nor sufficient by itself.

2. Two-band (single-orbit) bounds in terms of coherence/entanglement

Let $C(\mathbf{k}) = 2 |v_A(\mathbf{k})v_B(\mathbf{k})|$ be the concurrence of the state at \mathbf{k} . Then

$$|\eta(\mathbf{k})| = 2 |\text{Re}(e^{i\theta} v_A v_B^*)| \leq C(\mathbf{k}) \leq 1,$$

with equality $|\eta| = C$ when the witness phase is aligned with the A/B coherence. Using (32) and (28) gives the bounds

$$|\text{Im } \mathcal{Q}_{ij}^{(S)}| \leq \frac{C(\mathbf{k})}{2} |F_{ij}|, \quad |\mathcal{F}_{\lambda\lambda}^{Q,(S)}| \leq C(\mathbf{k}) \mathcal{F}_{\lambda\lambda}^Q. \quad (35)$$

In particular, if the state is separable at \mathbf{k} (i.e. $C(\mathbf{k}) = 0$), then $\mathcal{Q}_{ij}^{(S)}(\mathbf{k}) = 0$ and $\mathcal{F}_{\lambda\lambda}^{Q,(S)}(\mathbf{k}) = 0$ for any witness S , as desired. Summing (35) on an FHS mesh and applying Cauchy-Schwarz inequality, the upper bound of ν_S (33) is given as

$$|\nu_S| \leq \frac{1}{2\pi} \left(\sum_{\square} |F| \right)^{1/2} \left(\sum_{\square} C(\mathbf{k})^2 |F| \right)^{1/2}. \quad (36)$$

From (27), $g_{\lambda\lambda} = \frac{1}{4} |\partial_\lambda \hat{n}|^2$ and

$$|\partial_\lambda(v_A v_B^*)| \leq \frac{1}{2} |\partial_\lambda \hat{n}| = \sqrt{g_{\lambda\lambda}},$$

so, using (28), variations of the complex A/B coherence are controlled by the QFI:

$$|\partial_\lambda(v_A v_B^*)| \leq \frac{1}{2} \sqrt{\mathcal{F}_{\lambda\lambda}^Q}, \quad |\eta(\mathbf{k})| \leq C(\mathbf{k}) = \sqrt{1 - \hat{n}_z(\mathbf{k})^2}. \quad (37)$$

Equations (35)-(37) quantify the intuition that large S -filtered responses require regions where both the curvature and the FS metric are appreciable (e.g. Dirac vicinities in the Haldane phase diagram), and they vanish in parameter regions where the one-particle state is separable.

In the two-band case, equality in (34) occurs if and only if $|\eta| = 1$. With $S' = -\cos\theta\sigma_x + \sin\theta\sigma_y$, this means $n_z(\lambda) = 0$ and $\arg(v_A v_B^*) = -\theta$, i.e. $|v_A| = |v_B| = 1/\sqrt{2}$, therefore concurrence $C = 1$ and the state is maximally entangled. We randomly sample interior \mathbf{k} points from the BZ boundary and plot $(\mathcal{F}_\lambda^Q, \mathcal{F}_\lambda^{Q,(S)})$ in Fig. 1 (h). All points lie below the $y = x$ line, confirming $\mathcal{F}^{Q,(S)} \leq \mathcal{F}^Q$ (eq. (34)) and the linear control by $\|P^\perp S' P^\perp\|$.

3. Multi-orbital generalization

Let $\dim \mathcal{H}_A = m$, $\dim \mathcal{H}_B = n$ and consider a state $|\Psi_{\mathbf{k}}\rangle$ and a matrix J_F as eq. (20). Choose a unit pair $(x, y) \in \mathbb{C}^m \times \mathbb{C}^n$ and set the Bloch-space representative

$$S' = -\begin{pmatrix} 0 & Y \\ Y^\dagger & 0 \end{pmatrix}, \quad Y := xy^\dagger, \quad \|Y\|_{\text{op}} = 1. \quad (38)$$

Consider $\mathcal{Q}_{ij}^{(S)}$ (30). Since $P^\perp S' P^\perp$ is a Hermitian contraction on the conduction space,

$$\begin{aligned} |\mathcal{Q}_{ij}^{(S)}| &\leq \|P^\perp S' P^\perp\| \sqrt{g_{ii} g_{jj}}, \\ \mathcal{F}_{\lambda\lambda}^{Q,(S)} &:= 4 \operatorname{Re} \mathcal{Q}_{\lambda\lambda}^{(S)} \leq 4 \|P^\perp S' P^\perp\| g_{\lambda\lambda} \leq \mathcal{F}_{\lambda\lambda}^Q. \end{aligned} \quad (39)$$

With (38), $\|P^\perp S' P^\perp\| \leq \|S'\| = \|Y\|_{\text{op}} = 1$. While maximal entanglement indicates that substantial quantum resources are present, equality $\mathcal{F}^{Q,(S)} = \mathcal{F}^Q$ requires that the direction of parameter-induced change $v_\lambda := P^\perp \partial_\lambda u_-$ lie entirely in the $+1$ eigenspace of the compressed witness $T := P^\perp S' P^\perp$. Whenever v_λ has components along conduction directions on which T acts with eigenvalue < 1 (i.e., outside the S -selected channel), $\mathcal{F}^{Q,(S)}(\lambda)$ strictly falls below $\mathcal{F}^Q(\lambda)$, even for maximally entangled states. This is a crucial distinction from the single-orbit case, where the maximally entangled state gives the sufficient and necessary condition for the equality.

The negativity of the state (20) is $\|a(\mathbf{k})\| \|b(\mathbf{k})\|$. Using $\langle u_- | S' | u_- \rangle = -2 \operatorname{Re}(a^\dagger Y b)$ and the Cauchy-Schwarz inequality, we obtain

$$\begin{aligned} |\langle u_- | S' | u_- \rangle| &\leq 2 \|Y\|_{\text{op}} \|a\| \|b\|, \\ |\operatorname{Im} \mathcal{Q}_{ij}^{(S)}| &\leq \|Y\|_{\text{op}} \|a\| \|b\| |F_{ij}|. \end{aligned} \quad (40)$$

Thus, in higher local dimension the curvature $Q^{(S)}$ is simultaneously controlled by the witness strength $\|Y\|_{\text{op}}$ and the available entanglement $\|a\| \|b\|$.

V. Conclusion and Discussion

This work tests the proposal that quantum entanglement functions as a cohomological obstruction to assembling a global quantum state from locally compatible data, as formulated in [1]. We adopted the spinless Haldane model as a testbed and used a formulation

in which the occupied Bloch spinor at each crystal momentum is embedded into a single-excitation bipartite space. Within this setting we used exact lattice identities on a Fukui-Hatsugai-Suzuki mesh that relate the Chern number to witness-filtered sector integrals. The numerics confirm that the scalar response is governed by the curvature-weighted coherence and that the equal split construction isolates the coherent contribution carried by the off-diagonal sublattice amplitudes.

Mass sweeps across the topological and trivial regimes reproduce the expected plateau structure of the Chern number and verify the discrete identities. Two witness and three witness tomography recover the full phase dependence of the graded response from a minimal set of settings. These reconstructions track the complex amplitude that couples Berry curvature to sublattice coherence and remain stable under changes of the sampling mesh and gauge choices.

We extended the analysis to multi orbital embeddings. In that case the curvature-weighted coherence becomes a matrix and equal split rank one witnesses probe matrix entries through simple sinusoidal scans in the witness phase. The observed Levi types are controlled by the rank of the off-diagonal witness block, which fixes the sign ranks of the restricted sign operator and determines the structure group on the reduced bundle. The S -filtered geometric response satisfies sharp bounds. We also introduced the S -filtered QFI and explored its relation to the conventional QFI. These results show that the witness filter cleanly resolves the portion of the geometric response supported by inter-orbital or inter-sublattice coherence, which implies that sheafification preserves within patches while discarding global obstructions.

The consistency between analytical expectations and numerical results validates the use of witness-filtered constructions for probing entanglement, viewed as a geometric obstruction.

The present study can be extended to interacting models where the entanglement obstruction viewpoint is tested with projected many-body states and with numerically controlled approximations that preserve gauge structure. A systematic analysis of disorder and spatial inhomogeneity would clarify the stability of witness-filtered responses and of the sector identities away from translation invariance. Mixed state geometry offers another interesting avenue [28–30], through finite-temperature and dephasing studies that compare the filtered QGT and QFI with their counterparts on the twist torus. Multi-orbital and degenerate bands invite a non-Abelian treatment of the filtered connections, with direct tests of rank changes and Levi type across stratification walls, and with controlled comparisons to Hecke modifications. Higher-dimensional topological phases and driven settings can probe how the obstruction and the filtered responses behave under pumping and under periodic protocols. On the numerical side, adaptive Brillouin meshes and higher-order link formulas can bound discretization errors while enabling near-experimental re-

constructions of the curvature-weighted coherence matrix in cold-atom and photonic simulators. These extensions would strengthen the connection to the geometric Langlands picture [31–34] (and its relation to physics [35, 36]) and test the generality of entanglement as a cohomological obstruction in condensed matter realizations.

Acknowledgment

The first-named author is supported by the NSF, Office of Strategic Initiatives, under Grant No. OSI-2328774. The second-named author is supported by a Natural Sciences and Engineering Research Council of Canada (NSERC) Discovery Grant.

[1] K. Ikeda, “Quantum Entanglement as a Cohomological Obstruction,” [arXiv:2511.04326 \[math-ph\]](https://arxiv.org/abs/2511.04326).

[2] D. Xiao, M.-C. Chang, and Q. Niu, “Berry phase effects on electronic properties,” *Rev. Mod. Phys.* **82** (Jul, 2010) 1959–2007. <https://link.aps.org/doi/10.1103/RevModPhys.82.1959>.

[3] M. Z. Hasan and C. L. Kane, “Colloquium: Topological insulators,” *Rev. Mod. Phys.* **82** (Nov, 2010) 3045–3067. <https://link.aps.org/doi/10.1103/RevModPhys.82.3045>.

[4] X.-L. Qi and S.-C. Zhang, “Topological insulators and superconductors,” *Rev. Mod. Phys.* **83** (Oct, 2011) 1057–1110. <https://link.aps.org/doi/10.1103/RevModPhys.83.1057>.

[5] J. Maciejko and S. Rayan, “Hyperbolic band theory,” *Science Advances* **7** no. 36, (2021) eabe9170, [arXiv:2008.05489](https://arxiv.org/abs/2008.05489).

[6] E. Kienzle and S. Rayan, “Hyperbolic band theory through Higgs bundles,” *Advances in Mathematics* **409** (2022) 108664.

[7] J. Maciejko and S. Rayan, “Automorphic Bloch theorems for hyperbolic lattices,” *Proceedings of the National Academy of Sciences* **119** no. 9, (2022) e2116869119, [arXiv:2108.09314](https://arxiv.org/abs/2108.09314).

[8] K. Ikeda, S. Aoki, and Y. Matsuki, “Hyperbolic band theory under magnetic field and Dirac cones on a higher genus surface,” *J. Phys. Condens. Matter* **33** no. 48, (2021) 485602, [arXiv:2104.13314 \[cond-mat.mes-hall\]](https://arxiv.org/abs/2104.13314).

[9] K. Ikeda, Y. Matsuki, and S. Aoki, “Algebra of hyperbolic band theory under magnetic field,” *Canadian Journal of Physics* **101** no. 11, (2023) 630–640, <https://doi.org/10.1139/cjp-2022-0145>, <https://doi.org/10.1139/cjp-2022-0145>.

[10] I. Boettcher, A. V. Gorshkov, A. J. Kollár, J. Maciejko, S. Rayan, and R. Thomale, “Crystallography of hyperbolic lattices,” *Physical Review B* **105** no. 12, (2022) 125118, [arXiv:2105.01087](https://arxiv.org/abs/2105.01087).

[11] Á. Nagy and S. Rayan, “On the hyperbolic Bloch transform,” *Annales Henri Poincaré* **25** no. 3, (2024) 1713–1732, [arXiv:2208.02749](https://arxiv.org/abs/2208.02749).

[12] A. J. Kollár, M. Fitzpatrick, and A. A. Houck, “Hyperbolic lattices in circuit quantum electrodynamics,” *Nature* **571** no. 7763, (July, 2019) 45–50, [arXiv:1802.09549 \[quant-ph\]](https://arxiv.org/abs/1802.09549). <https://www.nature.com/articles/s41586-019-1348-3>.

[13] X. Xu, A. A. Mahmoud, N. Gorgichuk, R. Thomale, S. Rayan, and M. Mariantoni, “A scalable superconducting circuit framework for emulating physics in hyperbolic space,” [arXiv:2510.23827](https://arxiv.org/abs/2510.23827).

[14] S. Abramsky and A. Brandenburger, “The sheaf-theoretic structure of non-locality and contextuality,” *New J. Phys.* **13** no. 11, (2011) 113036, [arXiv:1102.0264 \[quant-ph\]](https://arxiv.org/abs/1102.0264).

[15] B. M. Terhal, “Detecting Quantum Entanglement,” *Theor. Comput. Sci.* **287** (2002) 313–335, [arXiv:quant-ph/0101032](https://arxiv.org/abs/quant-ph/0101032).

[16] O. Gühne and G. Tóth, “Entanglement detection,” *Phys. Rept.* **474** (2009) 1–75, [arXiv:0811.2803 \[quant-ph\]](https://arxiv.org/abs/0811.2803).

[17] G. Vidal and R. F. Werner, “Computable measure of entanglement,” *Phys. Rev. A* **65** (Feb, 2002) 032314. <https://link.aps.org/doi/10.1103/PhysRevA.65.032314>.

[18] A. Peres, “Separability criterion for density matrices,” *Phys. Rev. Lett.* **77** (Aug, 1996) 1413–1415. <https://link.aps.org/doi/10.1103/PhysRevLett.77.1413>.

[19] T. Fukui, Y. Hatsugai, and H. Suzuki, “Chern numbers in a discretized Brillouin zone: Efficient method to compute (spin) Hall conductances,” *J. Phys. Soc. Jap.* **74** (2005) 1674–1677, [arXiv:cond-mat/0503172](https://arxiv.org/abs/cond-mat/0503172).

[20] A. Uhlmann, “Parallel transport and “quantum holonomy” along density operators,” *Reports on Mathematical Physics* **24** no. 2, (1986) 229–240. <https://www.sciencedirect.com/science/article/pii/0034487786900558>.

[21] D. Bures, “An extension of kakutani’s theorem on infinite product measures to the tensor product of semifinite w^* -algebras,” *Transactions of the American Mathematical Society* **135** (1969) 199–212. [http://www.jstor.org/stable/1995012](https://www.jstor.org/stable/1995012).

[22] K. Ikeda, “Quantum Hall Effect and Langlands Program,” *Annals Phys.* **397** (2018) 136–150, [arXiv:1708.00419 \[cond-mat.mes-hall\]](https://arxiv.org/abs/1708.00419).

[23] K. Ikeda, “Topological aspects of matters and Langlands program,” *Rev. Math. Phys.* **36** no. 04, (2024) 2450005, [arXiv:1812.11879 \[cond-mat.mes-hall\]](https://arxiv.org/abs/1812.11879).

[24] F. D. M. Haldane, “Model for a quantum hall effect without landau levels: Condensed-matter realization of the “parity anomaly”,” *Phys. Rev. Lett.* **61** (Oct, 1988) 2015–2018. <https://link.aps.org/doi/10.1103/PhysRevLett.61.2015>.

[25] J. P. Provost and G. Vallee, “Riemannian structure on manifolds of quantum states,” *Commun. Math. Phys.* **76** (1980) 289–301.

[26] W. K. Wootters, “Statistical distance and hilbert space,” *Phys. Rev. D* **23** (Jan, 1981) 357–362. <https://link.aps.org/doi/10.1103/PhysRevD.23.357>.

[27] S. L. Braunstein and C. M. Caves, “Statistical distance and the geometry of quantum states,” *Phys. Rev. Lett.* **72** (May, 1994) 3439–3443. <https://link.aps.org/doi/10.1103/PhysRevLett.72.3439>.

[28] Z. Huang and D. P. Arovas, “Topological indices for open and thermal systems via uhlmann’s phase,” *Phys. Rev. Lett.* **113** (Aug, 2014) 076407. <https://link.aps.org/doi/10.1103/PhysRevLett.113.076407>.

[29] O. Viyuela, A. Rivas, and M. A. Martin-Delgado, “Uhlmann phase as a topological measure for one-dimensional fermion systems,” *Phys. Rev. Lett.* **112** (Apr, 2014) 130401. <https://link.aps.org/doi/10.1103/PhysRevLett.112.130401>.

[30] M. Hübner, “Computation of Uhlmann’s parallel transport for density matrices and the Bures metric on three-dimensional Hilbert space,” *Physics Letters A* **179** no. 4-5, (Aug., 1993) 226–230.

[31] D. Gaitsgory and S. Raskin, “Proof of the geometric langlands conjecture i: construction of the functor,” *arXiv:2405.03599* (2024) .

[32] D. Arinkin, D. Bernaldo, J. Campbell, L. Chen, J. Faergeman, D. Gaitsgory, K. Lin, S. Raskin, and N. Rozenblyum, “Proof of the geometric langlands conjecture ii: Kac-moody localization and the fle,” *arXiv:2405.03648* (2024) .

[33] J. Campbell, L. Chen, J. Faergeman, D. Gaitsgory, K. Lin, S. Raskin, and N. Rozenblyum, “Proof of the geometric langlands conjecture iii: compatibility with parabolic induction,” *arXiv:2409.07051* (2024) .

[34] D. Arinkin, D. Bernaldo, L. Chen, J. Faergeman, D. Gaitsgory, K. Lin, S. Raskin, and N. Rozenblyum, “Proof of the geometric Langlands conjecture IV: ambidexterity,” *arXiv:2409.08670* (2024) .

[35] A. Kapustin and E. Witten, “Electric-Magnetic Duality And The Geometric Langlands Program,” *Commun. Num. Theor. Phys.* **1** (2007) 1–236, [arXiv:hep-th/0604151](https://arxiv.org/abs/hep-th/0604151).

[36] E. Frenkel, “Lectures on the Langlands program and conformal field theory,” in *Les Houches School of Physics: Frontiers in Number Theory, Physics and Geometry*, pp. 387–533. 2007. [arXiv:hep-th/0512172](https://arxiv.org/abs/hep-th/0512172).